Use of radiation trapping for measuring electron-impact excitation cross sections for higher resonance levels of rare-gas atoms

M. D. Stewart, Jr., J. Ethan Chilton, John B. Boffard, and Chun C. Lin
Department of Physics, University of Wisconsin, Madison, Wisconsin 53706
(Received 19 September 2001; published 5 February 2002)

Radiation trapping causes the optical emission cross sections for transitions from an atomic resonance level to lower levels to be dependent on the atom number density. We have measured the optical emission cross sections for a number of heavy rare-gas resonance transitions over the pressure range of 0.04 to 30 mTorr. We compare the results with the theory of Heddle, using it to extrapolate our cross-section data to the high-pressure regime where the resonance radiation is completely reabsorbed. This allows us to obtain the apparent excitation cross section for seven resonance levels of Ne, Ar, and Kr without measuring the resonance radiation that would otherwise entail vacuum ultraviolet radiometry. In some cases, our analysis of the measured pressure dependence of the optical emission cross sections points out the need for improved transition probabilities values.

DOI: 10.1103/PhysRevA.65.032704 PACS number(s): 34.80.Dp, 34.80.My

I. INTRODUCTION

Measurement of electron-impact excitation cross sections by means of the optical method has been a research area of continued interest for decades, and has provided data that are important both to the basic understanding of electron-atom interaction and to technological applications. In a typical experiment a monoenergetic electron beam is incident on the target atoms. Radiation from atoms excited by the incident electrons is utilized to determine the excitation cross sections. By monitoring radiation of different frequencies it is possible to study the cross sections for a large number of excited states.

This paper is concerned with excitation into levels that are optically allowed to decay to the ground state. In principle, any level that can decay via electric-dipole selection rules to the ground state of an atom might be referred to as a ''resonance level'' [1,2]. However, in both historical and common usage, the term ''resonance level'' is reserved for describing only the lowest resonance levels with the strongest resonance transitions [3,4]. To preserve this historical distinction, in this paper we will refer to the higher resonance levels (i.e., ones other than the principal resonance levels) as *resonant* levels. Since, for the rare gases, the wavelength of the ground-state decay channel is in the far ultraviolet for all resonance levels, cross-section measurements of such levels are complicated by a unique set of experimental challenges. Numerous measurements have been made of the principal resonance transitions, $np^5(n+1)s(J=1)\rightarrow np^6(J=0)$, in the heavy rare gases (see review [5], as well as other works [6–11]). The accuracy of these measurements is limited by difficulties of the extreme-ultraviolet nature (xuv) of the transitions: Ne (73.6, 74.4 nm), Ar (104.8, 106.7 nm) and Kr(116.5, 123.6 nm). To circumvent the problem of working in the xuv, laser-induced fluorescence has also been used to study some of these levels [12].

In contrast to an atom in the principal resonance level which can decay only to the ground level, an atom excited to a higher resonant level may radiatively decay to the ground level *or* another lower level. For example, a resonant level in the $2p^5 3d$ configuration of neon (the $3d_2$ in Paschen's notation) can decay to either the $2p^6$ ground state, with a transition of 87.6 nm, or to the nine levels of the $2p^5 3p$ configuration with $J=0,1,2$ and transition wavelengths between 995 nm and 1.84 μm. The relative intensities of the various decay channels are governed by the branching fractions. Reabsorption of the radiation for the transition into the ground level by a nearby ground-level atom and the subsequent radiative decay result in a redistribution of the relative intensities among the various channels. Since the likelihood of reabsorption increases with the atom density, the observed branching fractions appear to vary with the gas pressure. This gives rise to a pressure dependence of the measured optical emission cross section that causes complications in determining excitation cross sections from optical studies [13,14].

The effects of reabsorption (also referred to as radiation trapping or imprisonment) of resonance radiation on optical measurements of electron-impact excitation cross sections have been extensively analyzed by Gabriel and Heddle [15] and by Heddle and Samuel [16]. They have derived an expression for the pressure dependence of the optical emission cross section measured at different pressures. Their results exhibit the expected two-limit behavior; i.e., at very low pressures reabsorption of resonance radiation is negligible and does not affect the emission cross sections, whereas at high pressures the measured emission cross section increases toward an asymptotic value. They verified experimentally the predicted pressure dependence for the case of He ($3^1P \rightarrow 2^1S$) emission.

Recent studies of electron-impact excitation of the heavy rare-gas atoms also reveal similar pressure dependence of the measured optical cross sections for emission from both resonant and nonresonant levels [13,17,18]. Nonresonant levels, which are not optically coupled to ground, are not expected to have pressure-dependent branching fractions. However, the emission cross sections from nonresonant levels exhibit pressure dependence due to the population of these levels by

cascades from resonant levels [13,14,17,18].

A detailed understanding of the effects of radiation trapping is essential for experimental measurements of the excitation cross sections for both resonant and nonresonant levels. In this paper we present cross-section data obtained as a function of pressure for emissions from resonant levels of Ne, Ar, and Kr, and analyze them in the framework of the Heddle model. This analysis allows us to obtain apparent excitation cross-section results without the need for xuv radiometry, which in the past has severely limited measurement of these cross sections [5]. The following section briefly reviews the optical method, and is followed by a description of the Heddle model. In Sec. III, we describe our technique to extract cross sections from the measured pressure dependencies of the data, and in Sec. IV we present our results.

II. THEORY

A. Optical method for measuring excitation cross sections

The principle, upon which the optical method is based, is that in steady state the rate of production of an excited atomic level is equal to the decay rate out of the level. The production rate is proportional to the excitation cross section, while the decay rate is equal to the photon flux of all transitions out of the level. The difficulty of applying the optical method is the necessity of detecting all photons emitted by an atom over a potentially very wide range of wavelengths. Since the optical method has been described at length in the literature [19], only a brief summary is given here to set forth the definitions and provide some remarks relevant to this paper.

An electron beam with current I traversing a gas inside a collision chamber with atom number density n_0 excites some of the atoms into energy level a that subsequently decays into a lower level b. The number of photons emitted in the $a \rightarrow b$ transition per unit time per unit beam length, Φ_{ab}, is measured and the optical emission cross section for this transition is defined as

$$Q_{ab}^{opt} = \frac{\Phi_{ab}}{(I/e)n_0}, \tag{2.1}$$

where e is the magnitude of the electron charge. If we measure the transitions from a level of interest into all the lower-lying levels, the sum of the optical emission cross sections is termed the ''apparent excitation cross section,''

$$Q_a^{app} = \sum_{b<a} Q_{ab}^{opt}, \tag{2.2}$$

which is a measure of the total rate of producing atoms in level a. At low pressures an excited level is populated by direct electron-impact excitation and cascades from the higher levels excited by the electron beam. The cascade cross sections can be determined by measuring the optical cross sections for transitions into the level a from the levels above it,

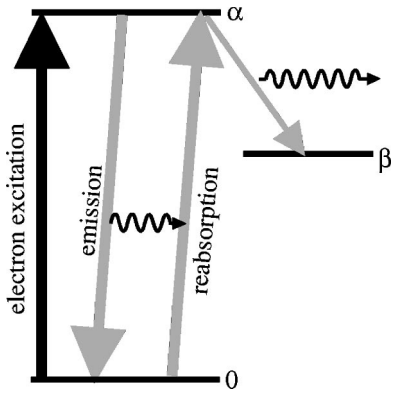

FIG. 1. Process of radiation trapping. An atom excited by electron-impact excitation into a resonant level, α, can decay to either the ground state, 0, or to some other level, β. At very high pressures, any photons emitted in the $\alpha \rightarrow 0$ transition will be reabsorbed by another atom before the photon leaves the collision region, resulting in an increased chance of a photon being emitted on the $\alpha \rightarrow \beta$ transition.

$$Q_a^{casc} = \sum_{c>a} Q_{ca}^{opt}. \tag{2.3}$$

The direct electron-impact excitation cross section is then equal to the difference between the apparent and cascade cross sections

$$Q_a^{dir} = Q_a^{app} - Q_a^{casc}. \tag{2.4}$$

The wide range of wavelengths [xuv to far-infrared(far-ir)] required to measure both the apparent and cascade cross sections has limited the applicability of the optical method in many cases. As an example, our recent measurements of electron excitation of the rare gases [13,17,18,20] extended from visible/near-uv to ir wavelengths, but not to the xuv. Thus, we reported no apparent cross sections for the resonant levels.

B. Model of radiation trapping

Consider an atom in a resonant level α which can decay either into the ground level, 0, or the nonresonant level β as illustrated in Fig. 1. Absorption of the resonant photons from the $\alpha \rightarrow 0$ transition by some other atom in its ground state generates another excited atom, which provides an additional opportunity for the $\alpha \rightarrow \beta$ transition. At higher gas pressures, the resonant radiation is more likely to be reabsorbed before the photon can escape the collision chamber so that the net result is to increase the branching fraction of the $\alpha \rightarrow \beta$ channel at the expense of the $\alpha \rightarrow 0$ channel. Thus, the optical cross section for the $\alpha \rightarrow \beta$ emission increases with pressure until it reaches a high-pressure limit when the $\alpha \rightarrow 0$ resonant radiation is completely reabsorbed.

Gabriel and Heddle [15] and Heddle and Samuel [16] have analyzed the effects of this radiation trapping on the pressure dependence of the $\alpha \rightarrow \beta$ emission cross sections. In their model, based on the earlier works of Holstein [2,21] and Phelps [22], radiation trapping is described by the frac-

tion of resonant photons escaping the collision chamber. This quantity [22], denoted by g, is a universal function of the dimensionless quantity $k_0\rho$. Here ρ is the characteristic collision radius for the geometry of the collision chamber and k_0 is the absorption coefficient of the resonant line, which is proportional to pressure as well as the transition probability of the $0\rightarrow\alpha$ transition. When the reabsorption of the $\alpha\rightarrow 0$ radiation and the subsequent production of the $\alpha\rightarrow\beta$ emission are taken into account, the optical excitation cross section for the $\alpha\rightarrow\beta$ transition at a pressure P, as defined in Eq. (2.1), becomes

$$Q_{\alpha\beta}^{opt}(P)=A_{\alpha\beta}\frac{Q_\alpha^{dir}+Q_\alpha^{casc}}{A'_\alpha+A_{\alpha 0}g[k_0(P)\rho]}, \tag{2.5}$$

where $A_{\alpha\beta}$ and $A_{\alpha 0}$ are the $\alpha\rightarrow\beta$ and $\alpha\rightarrow 0$ transition probabilities, respectively, and A'_α is the sum of the transition probabilities from the level α into all lower levels except the ground level. At very low pressures practically all the resonant photons escape the collision chamber without being reabsorbed and we have $g(k_0\rho)=1$. Equation (2.5) then reduces to the familiar expression relating the optical emission cross section to the apparent excitation cross section ($Q_\alpha^{dir}+Q_\alpha^{casc}$) and the branching fraction. At the other extreme of high pressures, $g(k_0\rho)$ approaches zero so that the $A_{\alpha 0}$ term disappears in Eq. (2.5), corresponding to complete trapping of the resonant radiation and eliminating the $\alpha\rightarrow 0$ channel for the decay of the level α.

III. METHOD

A. Apparatus

The apparatus used in this paper has been described in detail in our previous work [23], so only a brief overview is presented here. A stainless steel vacuum chamber is evacuated to a pressure of 10^{-8} Torr, then slowly backfilled with high purity gas ($>$99.999%). The pressure can be measured by either a capacitive manometer or a spinning rotor gauge. The electron gun contained within the collision chamber is composed of an indirectly heated BaO cathode, followed by multiple grids for electrostatic focusing and beam modulation. The electron-beam current is measured by a deep Faraday cup with an inner diameter of 2.1 cm. Fluorescence from excited atoms exit the collision region through two vertical slits cut in the Faraday cup.

Two different optical detector assemblies were used in this paper. For transitions in the visible spectrum (300–900 nm), a 1.26 m Czerny-Turner grating monochromator was used with a high sensitivity GaAs photomultiplier tube (PMT). For transitions beyond 900 nm, we used a Fourier-transform spectrometer (Nicolet model MagnaIR-860) operating in step-scan mode with either an $In_xGa_{x-1}As$ detector ($\lambda<1.6$ μm) or an InSb detector ($\lambda>1.6$ μm). Calibration procedures for both systems are described elsewhere [23].

B. Measurement of pressure curves

A sample plot of an optical emission cross section versus pressure is shown in Fig. 2. From Eq. (2.5) we see that the shape of the pressure curve for the optical cross sections depends on A'_α, $A_{\alpha 0}$, the universal function $g(k_0\rho)$, and the geometry parameter ρ. Although Q_α^{casc} may also be pressure dependent, its pressure dependence is neglected in the application of Heddle's model. This is because the cascades into the resonant level α come entirely from the nonresonant levels for which the reabsorption mechanism does not operate. These non-resonant levels, however, receive cascades from the higher resonant levels and such cascades are pressure dependent. Indeed the apparent excitation cross sections for nonresonant levels of the rare gases do exhibit pressure dependence, but to a much lesser extent than the resonant levels [13]. For the resonant levels the direct excitation cross sections generally dominate the cascade part, thus a modest pressure dependence in the Q_α^{casc} term in Eq. (2.5) constitutes only a small fractional contribution to $Q_{\alpha 0}^{opt}(P)$. Hence we neglect the pressure dependence of Q_α^{casc} in Eq. (2.5) as was done in Ref. [15]. This leads to a simplification that the pressure dependence is given entirely by the factor $[A'_\alpha+A_{\alpha 0}g(k_0\rho)]^{-1}$. Since $g(k_0\rho)$ tends to zero at high pressures and approaches one at very low pressures, the ratio of the cross sections at these two limits is

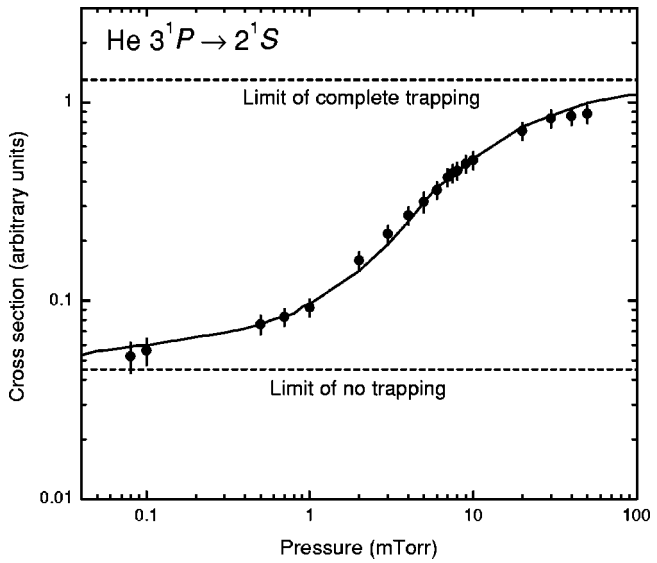

FIG. 2. Pressure curve for radiation trapping of He 3^1P resonant level at an electron-beam energy of 100 eV. At low pressures, most atoms excited to the 3^1P level decay to the ground state. At high pressures, radiation trapping of the resonance transition shifts almost all emissions to the $3^1P\rightarrow 2^1S$ transition. Line is fit of data to Eq. (2.5) with ρ as the only free parameter.

$$\frac{Q_{\alpha\beta}^{opt}(P\rightarrow\infty)}{Q_{\alpha\beta}^{opt}(P\rightarrow 0)}=1+\frac{A_{\alpha 0}}{A'_\alpha}. \tag{3.1}$$

To apply the Heddle model of radiation trapping to a particular system, one must have knowledge of the transition probabilities A'_α,$A_{\alpha 0}$ and the characteristic radius ρ. For helium the transition probabilities A'_α and $A_{\alpha 0}$ are well known [24], allowing us to extract the value of ρ from a least-squared fit of the measured values of $Q_{\alpha\beta}^{opt}(P)$ to Eq. (2.5).

Our fit yields a value of $\rho=(1.4\pm0.2)$ cm for both the He($5^1P\rightarrow2^1S$) and He($3^1P\rightarrow2^1S$) [shown in Fig. (2)] transitions and this value corresponds closely to the geometry of our apparatus. This value of ρ is adopted for the analysis of the other rare gases, since the same collision chamber is used for all measurements.

In comparison to helium, where the transition probabilities are well known, the situation for the heavier rare gases is rather different. Published values of theoretical calculations of transition probabilities are available [25–29], but the accuracy of these calculations is difficult to assess in view of the complexity of the atomic structure and the possible gross sensitivity of the transition matrix elements to the choice of the approximate wave functions. When comparing our measured $Q^{opt}(P)$ data to the results of Eq. (2.5) using published theoretical transition probabilities, there are varying levels of agreement. While some theoretical values fit our data well, in other cases we find a significant disagreement indicating the inaccuracy of the theoretical values of the transition probabilities.

An alternative approach is to treat $A_{\alpha0}$ and A'_α in Eq. (2.5) as parameters to fit the experimental data. As indicated by Eq. (3.1), $A_{\alpha0}/A'_\alpha$ is related to the ratio of the optical cross sections of the $\alpha\rightarrow\beta$ transition at the two asymptotic pressure limits. The magnitude of $A_{\alpha0}$ determines the degree of reabsorption. As we increase the pressure, the optical cross section $Q_{\alpha\beta}$ begins to increase over its low-pressure limit. The onset of this rise would shift to a lower pressure when $A_{\alpha0}$ becomes larger. Thus we preform a nonlinear least-squares fit of Eq. (2.5) to our measured $Q^{opt}(P)$ by adjusting $A_{\alpha0}$ and A'_α. This would provide an independent determination of the transition probabilities if there are enough data points over a pressure range extending to both the upper and lower asymptotic limits. However, practical reasons often restrict measurements of the optical emission cross sections to a limited pressure range. With limited data, it is often possible to obtain a satisfactory fit using different sets of values for $A_{\alpha0}$ and A'_α; i.e., different sets of $A_{\alpha0}$, A'_α, and $Q_{\alpha\beta}(P\rightarrow0)$ fit the observed data equally well. Under such circumstances, the fitted parameters may not represent a useful estimate of the transition probabilities. The quality of the fitted transition probabilities thus depends on the number of data points, the uncertainty in the values, and the pressure range they span. The relevance of these limitations on the extracted transition probabilities is discussed in Sec. IV C.

C. Determination of apparent excitation cross sections of resonant levels

At the high-pressure limit the $\alpha\rightarrow0$ decay channel is completely suppressed, so that the apparent excitation cross section for level α is the sum of the optical cross sections $Q^{opt}_{\alpha\beta}(P\rightarrow\infty)$ to all the lower levels β except the ground level, i.e.,

$$Q^{app}_\alpha=\sum_{\substack{\beta<\alpha\\ \beta\neq0}} Q^{opt}_{\alpha\beta}(P\rightarrow\infty). \tag{3.2}$$

All the transitions from the same upper level α have the same functional form of pressure dependence given by Eq. (2.5) except for a multiplicative constant. If we have the pressure curve for a particular transition from α, say $\alpha\rightarrow\beta_1$, we can use it to extrapolate all the cross sections measured at one pressure, P_1, to their high-pressure limits $Q^{opt}_{\alpha\beta}(P\rightarrow\infty)$ by the same scaling factor and obtain Q^{app}_α entirely from optical cross sections for the nonresonant emissions measured at one pressure P_1 according to

$$Q^{app}_\alpha=\frac{Q^{opt}_{\alpha\beta_1}(P\rightarrow\infty)}{Q^{opt}_{\alpha\beta_1}(P_1)}\sum_{\substack{\beta<\alpha\\ \beta\neq0}} Q^{opt}_{\alpha\beta}(P_1). \tag{3.3}$$

The $\alpha\rightarrow0$ emission is excluded in the above summation as the resonant radiation is completely reabsorbed and converted to other radiative channels at the high-pressure limit.

In Sec. III B, we indicated that the fitted parameters $A_{\alpha0}$ and A'_α may not correspond to accurate values of the transition probabilities because of the nonunique nature of fitting Eq. (2.5) to the experimental data. Fortunately, this reservation does not apply to the use of Eq. (3.3) to determine Q^{app}_α. This is because Eq. (3.3) is essentially an extrapolation from $P=P_1$ to $P\rightarrow\infty$. In this paper we limit the use of this procedure to cases where the measurements were made up to a sufficiently high pressure so that the extrapolation generally results in an increase of no more than 20%. In other words we use Eq. (2.5) as a quantitative method of extrapolation to obtain a small correction. Thus the analysis presented here allows us to determine the apparent cross sections for resonant levels without performing vacuum ultraviolet radiometry.

IV. RESULTS AND DISCUSSION

A. Comparison of pressure curves with Heddle's model

In Fig. 3, we plot our measured pressure dependence of the optical emission cross sections for ten resonant transitions of Ne, Ar, and Kr. The range of pressures is limited by poor signal rates at low pressures, and the possible onset of secondary effects at higher pressures. For the calculation of Heddle's model we start with theoretical values of $A_{\alpha0}$ and A'_α as the input to Eq. (2.5). All the A values for Kr were obtained from the calculation of Aymar and Coulombe [25]; the theoretical values needed for Ne and Ar were gathered from a number of different sources [26,27,29]. We will refer to these theoretical values collectively as the ''starting values.'' The modeled pressure dependence of Eq. (2.5) based on these starting input values is shown in Fig. 3 as dashed curves. In the alternative approach, fitting the experimental data to Eq. (2.5) to obtain values of $A_{\alpha0}$ and A'_α produces the solid curves in Fig. 3. Table I lists both the starting values (along with the source) and the fitted values for the ten transitions. In addition to the data shown in Fig. 3, we have measured pressure curves for an additional six resonant levels of Ne, Ar, and Kr. While we can fit the optical emission cross-section results for these levels to the Heddle model, the data points have not come close to approaching the high-pressure asymptote. These data are excluded from the

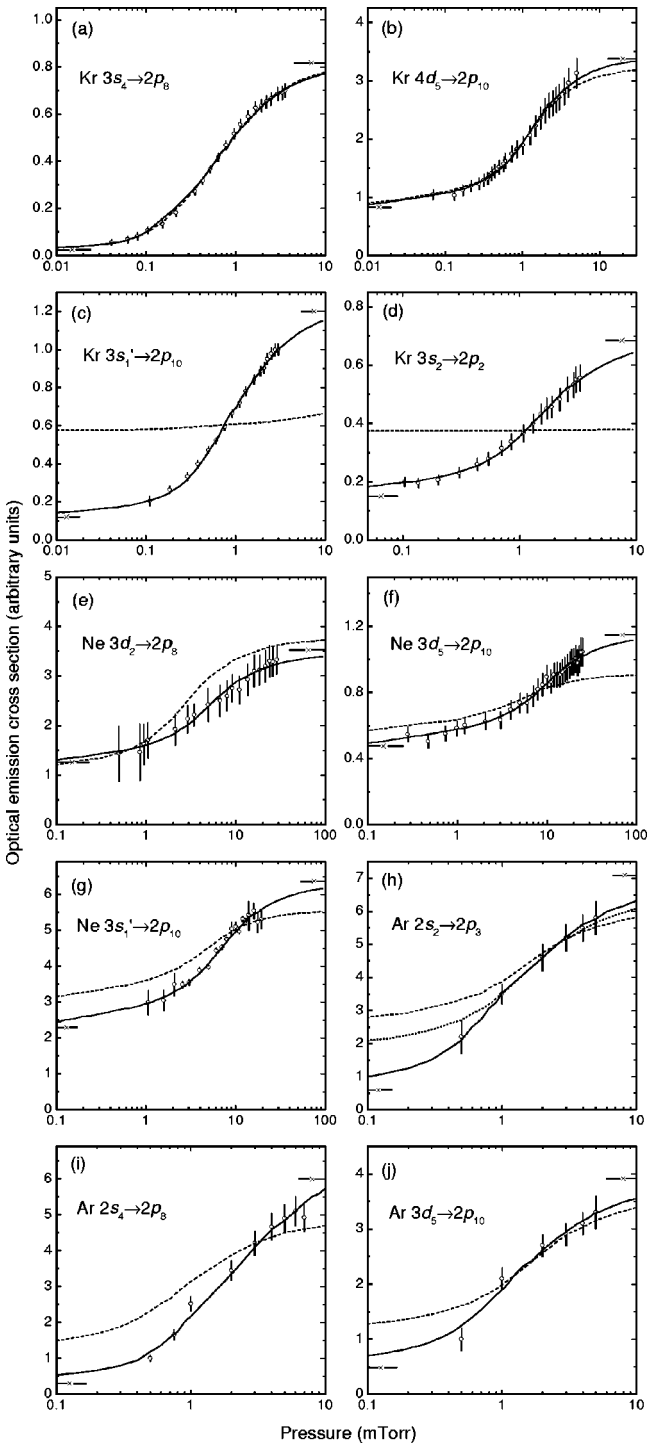

FIG. 3. Optical emission cross-section measurements (at 100 eV) as a function of gas pressure for selected resonant levels of Kr, Ne, and Ar. Dashed lines are modeled pressure dependencies using theoretical transition probabilities. Solid lines are results of fitting data to Eq. (2.5) by adjusting $A_{\alpha 0}$ and A'_{α}. Dotted line in (*h*) is best fit obtained by limiting the changes to the theoretical transition probabilities to $\pm 25\%$. Short segments labeled with an "$\times$" mark the high/low pressure asymptotic limits of the fitted curves.

TABLE I. Values of $A_{\alpha 0}$ and A'_{α} (in units of 10^7 s^{-1}). Starting values are theoretical numbers from the sources cited, fitted values are extracted from nonlinear least-squares fit of Eq. (2.5) to experimental measurements. Fits are nonunique, resulting in large uncertainties in fitted transition probabilities, i.e., $\geqslant 100\%$ except otherwise noted.

	$A_{\alpha 0}$		A'_{α}	
	Starting	Fitted	Starting	Fitted
Kr($3s_4$)	30 [a]	31 [b]	0.93 [a]	0.98 [b]
Kr($4d_5$)	2.8 [a]	2.6 [b]	1.0 [a]	0.85 [b]
Kr($3s_1'$)	0.21 [a]	7.3 [b]	0.85 [a]	0.81
Kr($3s_2$)	0.041 [a]	3.0 [b]	1.1 [a]	0.83
Ne($3d_2$)	9.3 [c]	3.2	3.7 [d]	1.8
Ne($3d_5$)	3.3 [c]	2.0	5.0 [d]	1.5
Ne($3s_1'$)	3.8 [c]	3.2	4.2 [d]	1.8
Ar($2s_2$)	3.5 [c]	12	2.02 [c]	1.3
Ar($2s_4$)	7.7 [c]	11	2.06 [c]	0.58
Ar($3d_5$)	3.5 [e]	7.8	1.4 [e]	1.1

[a]Reference [25].
[b]$\leqslant 50\%$ estimated uncertainty.
[c]Reference [26].
[d]Reference [27].
[e]Reference [29].

present paper since extrapolation by Eq. (3.3) to obtain the apparent excitation cross sections may entail a substantial uncertainty.

To discuss the individual cases, consider first the Kr($3s_4$) level. Inputting the starting values of $A_{\alpha 0}$ and A'_{α} (Table I) to Eq. (2.5) generates a curve that reproduces all the data points almost perfectly as shown in Fig. 3(a). Not surprisingly a least-squares fit of Eq. (2.5) to the experimental data gives practically the same fitted values as the starting values. Another strong case is the Kr($4d_5$) level in Fig. 3(b). The pressure curve generated by the starting *A* values agree very well with our measurements except for a slight underestimation at high pressure. Only a minor adjustment ($\leqslant 15\%$) of the *A* values is needed to optimize the fit.

In Figs. 3(c) and 3(d) we have the opposite situation, wherein the pressure curves derived from the starting values of the parameters are virtually flat and bear no resemblance to the experimental data. These starting values give the ratio $Q(P\rightarrow\infty)/Q(P\rightarrow 0)$ as 1.25 for Kr($3s_1'$) and 1.04 for Kr($3s_2$) which are much too small in comparison to our measurements. Fitting Eq. (2.5) to the observed values results in an order-of-magnitude increase in $A_{\alpha 0}$ but only a modest change in A'_{α} as listed in Table I. The change in $A_{\alpha 0}$ not only affects the high-to-low pressure limits, but also the effective pressure where reabsorption begins to manifest itself via the dependence of k_0 on $A_{\alpha 0}$. Since the four pressure curves in Figs. 3(a)–3(d) all start to increase in roughly the same pressure region, it is clear that starting values of $A_{\alpha 0}$ for the Kr($3s_1'$) and Kr($3s_2$) levels are too small. For these two levels our measurements provide a distinct improvement of the $A_{\alpha 0}$ value over the theoretical calculations.

For the Ne and Ar levels, Figs. 3(e)–3(j) show a varying degree of agreement between the experimental data and the calculated pressure dependence based on the starting values of the parameters. Generally, the fitted transition probability values for these levels are within a factor of two compared to the starting theoretical values. In Sec. IV C, we will discuss to what accuracy the fitted values can be taken as the transition probabilities.

With the fitted pressure curves we determine the two asymptotic cross sections, $Q(P\rightarrow\infty)$ and $Q(P\rightarrow 0)$. These values are marked on the graphs of Fig. 3. The upper asymptotic cross sections are of special importance for determining the apparent excitation cross sections as discussed in Sec. III C.

B. Alternative sources of pressure effects

While we can find possible transition probabilities to make our data fit the Heddle model, the validity of this method depends upon the assumption that radiation trapping is *the* sole cause of the pressure effects. In this section we attempt to support that assumption by eliminating the alternative causes.

A number of possible causes of observed pressure effects could be discarded by finding a level that has no pressure dependence, since this would rule out most experimental artifacts (such as nonlinearities in pressure measurement, PMT response, . . . ,). In the absence of cascades, radiation trapping to the $^1S_0$ ground state of the heavy rare gases would only affect energy levels with $J=1$ and odd parity. However, due to cascade transitions out of radiation trapped levels, pressure dependence can be passed to nonresonant levels. All levels receive cascades either directly from a resonant level (i.e., the krypton $4p^5 5p$ levels with $J=0,1,2$ from the $4p^5 6s$ and $4p^5 4d$ levels with $J=1$), or indirectly from levels that themselves receive cascades from resonant levels (i.e., the krypton $4p^5 4d$ levels with $J=0,2,3$ from the $4p^5 6p$ levels with $J=0,1,2$ which had received cascades from higher resonant levels such as the $4p^5 5d$ levels). The levels with the least expected pressure dependence are ones that receive cascades from resonant levels only through very indirect routes. For example, the first resonant levels that could possibly contribute cascades to the Ar $3p^5 4p$ $J=3$ level ($2p_9$) are the $J=1$ levels of the $3p^5 6s$ configuration: $3p^5 6s(J=1) \rightarrow 3p^5 5p(J=1,2) \rightarrow 3p^5 5s(J=2) \rightarrow 3p^5 4p(J=3)$. Due to the long, convoluted nature of this decay chain, the pressure effects for this level are minimal as we demonstrated in our earlier work [13]. Figure 4 is a pressure curve taken over the same range of pressures as our other curves for the Kr($2p_9$) level, whose cascade chain from a resonant level is similar to the Ar($2p_9$) level. While there is a small dependence on pressure, it is essentially constant over the range of pressures which show substantial pressure effects in the resonant levels.

Since some levels have little or no observable pressure effects, the cause(s) of pressure effects must not lie in the apparatus but within some parameter(s) of the collision physics that varies from one atomic level to another. For example, levels exhibit a range of lifetimes. As the pressure is increased, the diffusion length of atoms decreases, so long-lived atoms are less likely to diffuse away from the collision region. Resonant levels, however, generally have shorter lifetimes than nonresonant levels, so one would expect the diffusion-limiting effect to be less important for those levels where we observe the largest pressure effects.

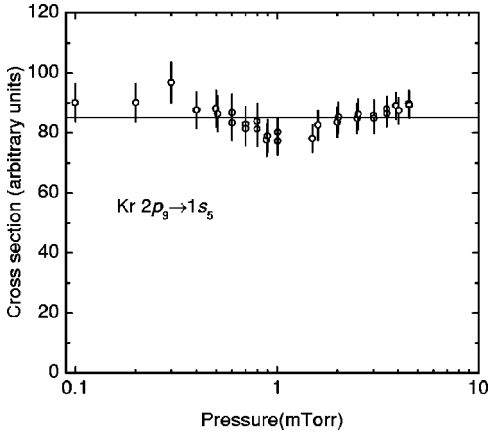

FIG. 4. The measured optical emission cross section for the nonresonant Kr $2p_9(J=3)$ level has no characteristic pressure dependence at 40 eV.

A possible cause of nonlinear signal dependence upon pressure is a state-selective population of excited levels via some secondary collision process. Examples of this class include: electron-metastable atom collisions [30], ion-atom collisions, or dissociative recombination of rare-gas eximers. These processes all rely on the electron beam creating some excited state/ion which then undergoes either an additional electron-atom collision or some other ion/atom-atom collision. Since the number of ions or excited atoms created in the first step is proportional to the electron-beam current as well as the pressure, the measured cross section from these processes should exhibit a linear dependence on pressure and electron-beam current. Since we observe an *s*-shaped pressure curve and no dependence of the cross section on electron-beam current, these processes do not fit our observations.

Other possible causes of pressure effects include the pressure dependence of polarization [31], stimulated emission [32], and collision transfer [15]. Heddle and Lucus [33] observed that the measured polarization of the fluorescence for excitation of helium levels decreases with increasing pressure. While some degree of this variation is due to radiation trapping, the general cause is collisions with background gas atoms that randomizes the preferred quantization axis imposed on the atoms by the electron's trajectory. In the worst case scenario of a starting polarization of 100% and complete collisional depolarization, this would amount to only a 33% pressure-dependent change in the cross-section results. In comparison to this theoretical maximum effect of 33%, the Kr($3s_1'$) level, where the use of theoretical transition probabilities in the Heddle model does a poor job, has an observed variation in a cross section of over 500%. So depolarization alone is insufficient at explaining our observations. In fact, with realistic values of starting polarization

(less than 10% at 100 eV) this effect would have no noticeable effect on our measurements. We do note, however, that any effect of depolarizing collisions would tend to improve the accuracy of our radiation trapping results by decreasing the effect of polarization.

DeJoseph and Clark [32] have raised the possibility of stimulated emission playing a potential role in pressure effects. Essentially, if the direct electron-impact cross sections into resonant levels (and thus the populations) are larger than the cross sections into the levels which the resonant levels decay to, a weak population inversion exists between the two levels which, in principle, could provide some gain to the transition connecting the levels. This process would lead to an *s*-shaped pressure curve since as the pressure is increased, the ''gain'' on the selected level would increase, resulting in a larger measured cross section; until the excited level was being depopulated solely through this stimulated-emission channel, at which point the measured optical emission cross section would level off. The condition necessary for this effect to be important is that the stimulated emission rate, $B_{ul}u(\nu_{lu})$, should be around the same order of magnitude as the spontaneous emission rate, A_{ul}. The radiation intensity required for this condition (on the order of mW/cm^2), however, is at least five orders of magnitude larger than the light levels produced in our experiment.

Collision transfer involves the transfer of energy from one excited state into another excited state via a collision with another atom (presumably in the ground state). At very high pressures (many Torr) excited levels are brought into a state of collision-induced equilibrium where the population of each state is proportional to the level's statistical weight. The pressure at which this collision transfer mechanism becomes important is determined by the excitation-transfer cross sections out of the relevant energy levels. The largest collision transfer cross sections are between atomic levels whose energies are less than kT apart in energy (208 cm^{-1} at room temperature). For example, in krypton the energy levels of the resonant $3d_2$ level and the $2s_5(J=2)$ level differ by only 19 cm^{-1}, and in neon the energies of the resonant $3s_1'(J=1)$ and $3s_1''(J=2)$ levels differ by only 16 cm^{-1}. These levels would be expected to have the largest collision transfer cross sections, and thus the lowest pressures where collision transfer effects would be important.

To discount the role of excitation transfer to the pressure effects we have attributed to radiation trapping, we have looked for the pressure onset of collision transfer effects for selected levels at much larger gas pressures than used elsewhere in this paper. To increase the sensitivity of these measurements, rather than looking for the small change in the resonance level depopulation, we have examined the enhancement in collision transfer in a nonresonant level. At 100 eV, the direct cross section into the Ne($3s_1''$) level is relatively small, whereas the cross section into the resonant Ne($3s_1'$) level is relatively large. At high pressures, excitation transfer will increase the small population of atoms in the $3s_1''$ level at the expense of the much larger number of atoms in the $3s_1'$ level. Indeed, we have seen such an enhancement in the $3s_1''\rightarrow 2p_{10}$ optical emission cross section, but the effect only starts to become significant above 20 mTorr. Since the pressure effects we report in this paper occur at much lower pressures, collision transfer is unable to explain our observed pressure effects.

C. Transition probabilities

In principle, the transition probabilities $A_{\alpha 0}$ and A_α' can be obtained from a fit of Eq. (2.5) to the observed pressure-dependence curve. The uniqueness of the resulting fit can be assured if the following three quantities are known: (1) the low-pressure limit of the cross section, (2) the high-pressure limit of the cross section, and (3) the pressure at which this transition between these two limits reaches the halfway point. These features set the two effective free parameters in Heddle's model: the ratio of the two limiting cross sections is related to $A_{\alpha 0}/A_\alpha'$ by Eq. (3.1), and the critical pressure determines the absorption coefficient (k_0 which is proportional to $A_{\alpha 0}$). In reality our measurements do not extend to the asymptotic limits. The ratio of our highest- to the lowest-measured cross section could be much smaller than $Q(P\rightarrow\infty)/Q(P\rightarrow 0)$ so that one cannot fix $A_{\alpha 0}/A_\alpha'$ directly from the raw data. Instead we have had to resort to least-squares fitting with $A_{\alpha 0}$ and A_α' as free parameters. This leads to a high degree of covariance between the fitted values of $A_{\alpha 0}$ and A_α'. This is particularly troublesome in cases where the limited amount of data does not display the asymptotic behavior.

For example, consider the Ar($2s_2\rightarrow 2p_3$) data shown in Fig. 3(h). The wavelength for this transition is 1.301 μm, which necessitated the use of low sensitivity ir detectors, which in turn limited the low-pressure limit with which we could obtain data. Due to the lack of low-pressure data, there is great uncertainty in $Q(P\rightarrow 0)$. The modeled pressure curve obtained from the starting values of the parameters, gives a high relative value for $Q(P\rightarrow 0)$, in poor agreement with our data. Starting from this theoretical pressure curve, a better fit is obtained by shifting the curve to the right and increasing the gap between the two extreme cross sections—both of which are obtained by increasing the value of $A_{\alpha 0}$. However, the data can be fit nearly equally as well by simply decreasing the value of A_α'. The best fit line in Fig. 3(h) is obtained with a mixture of these approaches, $A_{\alpha 0}$ is increased by 240%, while A_α' is decreased by 40%. The change in the value of $A_{\alpha 0}$ is well outside the $\pm 25\%$ uncertainty assigned to this transition probability, while the change in the value of A_α' is still within the $\pm 50\%$ effective uncertainty [26]. However, we can obtain a fit that is nearly as good by constraining the changes in both values to be within $\pm 25\%$ of the starting theoretical values [see dotted line of Fig. 3(h)]. The main differences in the resulting pressure curves occur at very low pressures where we have no data, the high-pressure limit of the cross sections show little change for the various fits. Since we are mainly concerned with the high-pressure limit of the data for the determination of apparent cross sections, the nonuniqueness of the fitted curves at low pressure (and thus the fitted transition probabilities) has little bearing on the cross sections (Sec. IV D) we obtain.

There are also a couple of additional physical processes that increase the difficulty in extracting accurate transition probabilities with this method [34,35]. In particular, there is some uncertainty in the value of the function $g(k_0\rho)$. At high pressures, the functional dependence of the g function varies slightly depending on where one assumes radiating atoms are located within the collision chamber [16]. Furthermore, the value of the absorption coefficient, k_0, also has some potential problems with it due to isotope effects [35]. For example, if more than one isotope is present in the gas, and the isotope shift for the transition is larger than the Doppler width, the effective value of k_0 will be less than the value used in our model calculations. Additionally, at very high rates of reabsorption (high pressures), it is necessary to use a Voight line shape, rather than the Doppler profile assumed in this analysis, to accurately model the resonance reabsorption process. The omission of these factors from the model, however, can be partially offset in the fitting of our results to the model by variations in the fitted parameters, namely $A_{\alpha 0}$ and A'_{α}. Hence, the modeled values at any given pressure have a much lower uncertainty than the uncertainty in the fitted values of $A_{\alpha 0}$ and A'_{α}.

Due to the wide range of potential values of $A_{\alpha 0}$ and A'_{α} that yield acceptable fits, the uncertainties in the fitted values of the transition probabilities are generally very large ($>100\%$). Our measurements of the pressure effects, however, clearly reveal the inadequacy of the calculated values of $A_{\alpha 0}$ for the Kr$(3s'_1)$ and Kr$(3s_2)$. Theoretical calculations of transition probabilities involving highly excited states are exceedingly difficult. The wave functions are complicated by possible configuration interactions with a vast number of states and the transition moments may vary sensitively with the oscillatory nature of the matrix element integrand. The transition probability parameters determined by indirect means as in this paper could be of considerable value in cases where clear asymptotic behavior (at both pressure limits) is displayed.

D. Cross sections for resonant levels

For seven of the levels listed in Table I we have measured all the emission lines out of the level, except for the transitions to the ground state. Combining these measurements with the ratios taken from the fitted pressure curves of Fig. 3 we obtain the apparent excitation cross sections in accordance with Eq. (3.3). In Fig. 5, we show the apparent excitation functions for the Ne$(3d_2)$,Ne$(3d_5)$,Ne$(3s'_1)$, and $Kr(3s'_1)$ levels. In the case of the Ar$(2s_2)$,Ar$(2s_4)$, and Ar$(3d_5)$ levels, we have also measured all of the significant cascade cross sections into these levels allowing us to obtain the direct cross sections via Eq. (2.4). The extrapolation made in the value of the cross sections from the highest measured pressure to the limit of complete radiation trapping is generally less than 20%. Thus, even with a 50% uncertainty in this extrapolation, the uncertainty introduced into our final cross-section results is less than 10%.

1. Neon and krypton

In a previous paper, we have determined the apparent excitation cross sections for the nonresonant levels ($J=0,2,3,4$) of the $2p^5 3d$ configuration of Ne [18]. For the $J=1$ resonant levels the transitions to the ground level are in the xuv and were not measured. However, the observed pressure curves [see Figs. 3(e)–3(g)] indicate that the reabsorp-

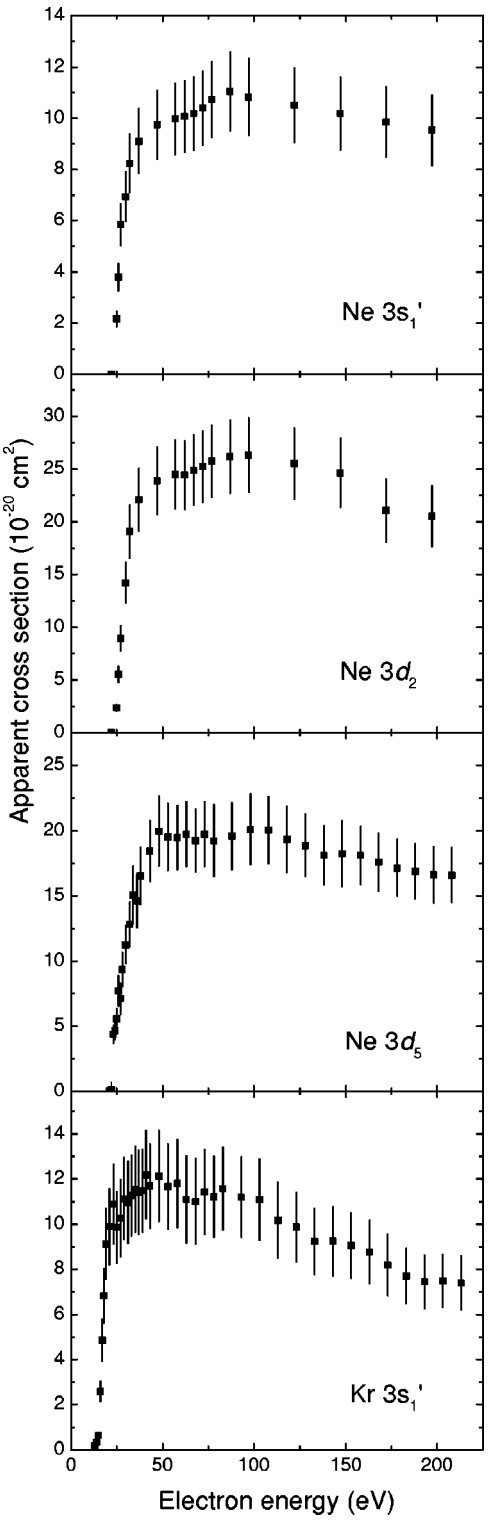

FIG. 5. Apparent cross-section results for Ne and Kr resonant levels. Error bars include systematic and statistical uncertainties, as well as the uncertainties introduced from extrapolating to the complete radiation-trapping domain.

tion is almost complete at 20 mTorr. Thus the sum of the optical cross sections for emission from the resonant levels into all the lower levels except the ground state measured at 20 mTorr was taken as an approximation to the apparent cross section in the paper by Chilton *et al.* [18]. The values we report here for the $3d_2$,$3d_5$, and $3s_1'$ levels are a result of applying the Heddle model to extrapolate the values to infinite pressure, and indeed are only 15% larger than the values reported in Ref. [18]. These results confirm that the resonant levels of the $2p^5 3d$ configuration have much larger cross sections than the nonresonant levels of the same configuration except near the energy threshold. Kanik, Ajello, and James [6] have measured the xuv emission cross sections of neon at an energy of 300 eV. They were unable to resolve the individual $2p^5 3d \rightarrow 2p^6$ emission lines, so they report only a sum cross section of $(32.9 \pm 13.5) \times 10^{-20}$ cm^2 (feature 5 of Table I in Ref. [6]). Since we only obtained data up to an electron energy of 200 eV, we use their $1s_2$ and $1s_4$ excitation functions as a guide to estimate from their data a value at an energy of 200 eV of $(41 \pm 18) \times 10^{-20}$ cm^2. In comparison, combining our present results for the three $2p^5 3d$ $J=1$ levels we obtain a sum of $(49 \pm 10) \times 10^{-20}$ cm^2 at 200 eV. Considering the extrapolation necessary to compare both data sets, this is remarkably good agreement.

In the case of Kr, apparent excitation cross sections for only three of the $4p^5 4d$ non-resonant levels ($3s_1''$,$3d_1''$,$3d_1'$) were reported in Ref. [17]. Again the cross sections for these three nonresonant level are smaller than the cross section of the resonant Kr($3s_1'$) level except near the onset energy.

Pressure curves for three additional krypton levels were included in Fig. 3, but no apparent excitation cross sections are presented. The $3s_2$ and $3s_4$ levels can decay to both the $2p$ and $3p$ Paschen levels. The transitions into the $3p$ levels range in wavelength from 1.2 μm to 5.0 μm. Due to low detector sensitivity, we have been unable to measure all of these transitions. According to the calculations of Aymar and Coulumbe [25], these transitions make up a significant fraction of the total decays out of these levels. Due to the larger uncertainty introduced from the estimation of the missing optical emission cross sections into the resulting apparent cross section, we do not present results for these two levels. We also do not present apparent cross-section results for the $4d_5$ level due to complications arising from the inability to resolve all of the emissions out of this level.

2. Argon

Due to argon's wide use in plasma processing, as well as it being the third most abundant gas in the earth's atmosphere, there has been much more work on the electron-impact excitation of the resonance and nonresonant levels of argon than the other rare gases. We have previously [23] measured all of the significant cascades into the $3p^5 5s$ and $3p^5 3d$ configurations, allowing us to obtain direct cross sections for all of the nonresonant levels in these configurations. The present radiation trapping method has allowed us to extend these measurements to three resonant levels: the $2s_2$ and $2s_4$ levels of the $3p^5 5s$ configuration, and the $3d_5$ level of the $3p^5 3d$ configuration.

TABLE II. Comparison of argon $3p^5 5s$ direct cross sections (in units of 10^{-19} cm^2). Results for the $2s_3$ and $2s_5$ levels are from Ref. [23]. Uncertainties are on the order of 25%.

	Energy (eV)		
	peak	50	100
$2s_2(J=1)$	12	9.2	7.7
$2s_3(J=0)$	5.4	1.1	0.15
$2s_4(J=1)$	25	23	21
$2s_5(J=2)$	24	4.8	0.94

At low energies, the direct excitation cross sections into the argon $2s_3$ and $2s_5$ non-resonant levels are comparable in size to the cross sections into the resonant $2s_2$ and $2s_4$ levels; in fact, the cross section into the $2s_5(J=2)$ level is twice as large as the direct cross section for the $2s_2$ level. At high electron energies, however, the resonant levels have much larger cross section as listed in Table II. In comparison to the broad energy dependence of the cross sections shown by the $2s_2$ and $2s_4$ levels in Fig. 6, the $3d_5$ level has a much sharper appearance even though all three levels are optically connected to the ground state. As described in our previous work [23] this is due to the singlet component in the wave function of the $3d_5$ level being unusually small. It is also noteworthy that the cascade contribution to the total apparent cross sections for these levels can be quite substantial; for example, the total cascades into the $2s_2$ level are 50% the size of the direct-excitation cross section even at 200 eV.

Mentall and Morgan have measured the xuv emission lines for these three argon lines at an electron energy of 200 eV [36]. We can convert our apparent cross sections into the uv optical emission cross sections (at zero pressure) by multiplying by the appropriate branching fractions. Thus, we interpolate from our data that the $2s_2 \rightarrow {}^1S_0$ optical emission cross section has a value of $(5.1 \pm 2.4) \times 10^{-19}$ cm^2, and the $2s_4 \rightarrow {}^1S_0$ emission line has a value of $(14 \pm 6) \times 10^{-19}$ cm^2 (where the large uncertainties arise mainly from the branching ratios). In comparison, Mentall and Morgan report a value of 7.3×10^{-19} cm^2 for the 880.0 Å($2s_2 \rightarrow {}^1S_0$) line, and 5.4×10^{-19} cm^2 for the 870.0 Å($2s_4 \rightarrow {}^1S_0$) line [36]. Due to improved measurements of the nitrogen line used by Mentall and Morgan for absolute calibration, however, it has been suggested that their results should be corrected by a factor of 0.61 [5]. With this correction, their values are $(4.4 \pm 0.9) \times 10^{-19}$ cm^2 for the $2s_2 \rightarrow {}^1S_0$ line, and $(3.3 \pm 0.7) \times 10^{-19}$ cm^2 for the $2s_4 \rightarrow {}^1S_0$ line. While we have good agreement for the $2s_2$ emission line, there is serious discrepancy on the value of the $2s_4 \rightarrow {}^1S_0$ optical emission cross section.

Ajello *et al.* [7] have also measured the xuv spectrum of argon at an electron energy of 200 eV. They were not able to fully resolve the $2s_2$ and $2s_4$ emission lines from the nearby $2p^5 3d$ resonant emission lines. They found the combined $2s_2 + 3s_1'$ uv-emission cross sections to be $(62 \pm 14) \times 10^{-19}$ cm^2, and the combined $2s_4 + 3d_2 + \cdots$ cross section to be $(75 \pm 17) \times 10^{-19}$ cm^2. Our results are well under

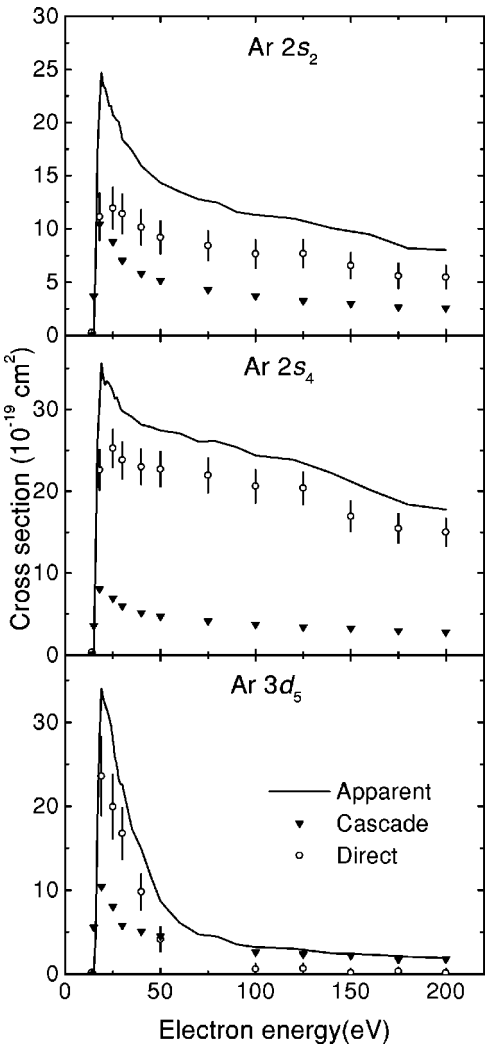

FIG. 6. Cross-section results for resonant levels of Ar. Error bars include systematic and statistical uncertainties, as well as the uncertainties introduced from extrapolating to the complete radiation-trapping domain.

the upper limits these measurements place on the $2s_2$ and $2s_4$ emission cross sections.

There have been a number of theoretical calculations of the cross sections for the argon resonant levels. A sampling of these values are provided in Table III. The calculation of Ref. [29] which is based on the distorted-wave Born approximation with exchange yields cross sections larger than the present results by 25% for the $2s_4$ level, a factor of 3 for the $2s_2$ level, and a much larger factor for the $3d_5$ level. The poor agreement for the $3d_5$ level can be easily explained by noting the sensitivity of the calculation on the very small singlet component of the wave function. However, it is interesting to note that the reasonable agreement for the $2s_4$ level and poor agreement for the $2s_2$ level is opposite to the experimental measurement of the uv optical emission lines by Ref. [36]. In comparison, the earlier plane-wave Born calculation of Peterson and Allen [37] is much closer to our observed values. Their calculation used generalized oscillator strengths extracted from experimental measurements of electron-impact energy-loss spectra (EELS). The incorporation of EELS experimental data in their semiempirical calculation may explain the much better agreement for the $3d_5$ level.

TABLE III. Comparison of direct cross sections (in units of 10^{-19} cm^2) for excitation into resonant levels of the argon $3p^5 5s$ and $3p^5 3d$ configurations at 100 eV.

	This paper	Semiempirical Born [37]	Distorted-wave approx. [29]
$2s_2$ $(5s'[1/2]_1)$	8 ± 2	8.8	21
$2s_4$ $(5s[3/2]_1)$	21 ± 3	27	25.6
$3d_5$ $(3d[1/2]_1)$	1 ± 0.7	1.8	11.5

An alternative means of absolute calibration of cross section for resonance levels is based upon normalizing results at high electron energies to the Born-Bethe approximation. At high energies, the direct excitation cross section is proportional to the oscillator strength of the corresponding optical transition. For example, McConkey and Donaldson [11] measured the cross sections for the Ar $1s_2$ and $1s_4$ resonance levels by normalizing their data from 400 eV to 2000 eV to the known oscillator strengths. The maximum energy of our data is only 200 eV, which is too low to reliably apply the Born-Bethe approximation. Nonetheless, the oscillator strengths derived from our data taken between 100 eV and 200 eV are consistent with the theoretical values. For the $2s_2$ and $2s_4$ levels we find *f*-values of 0.009 ± 0.003 and 0.027 ± 0.005 respectively, versus theoretical values of 0.012 and 0.027 [26].

V. CONCLUSIONS

We have demonstrated that radiation trapping can be used to measure the apparent cross sections for resonant levels without having to measure the difficult xuv emission lines. Furthermore, the measurements need not be taken at extremely high pressures since the Heddle model of radiation trapping can be used to extrapolate from workable pressures to the asymptotic limit. In this paper, we have presented results where the amount of this extrapolation was limited to a small correction from the highest measured pressure. In principle, the method could also be used in cases where the extrapolations are much larger if the transition probabilities were known with some certainty beforehand. Alternatively, if the pressure curves were extended to higher and lower pressures, the method could be used to obtain both apparent cross sections *and* transition probabilities. Unfortunately, at the moment the low end of our pressure curves are limited by the low signal rates (particularly for ir lines), while the high end of our pressure curves are limited by electron-beam defocusing effects and the possible onset of other secondary processes. In principle, these technical problems could be overcome with improved detectors, electron-gun designs, and the inclusion of collision transfer terms to the fitted model.

While the present approach of complete radiation trapping to remove the need to measure resonance transitions has enabled us to determine the excitation cross sections for several

resonant levels of Ne, Ar, and Kr, it is not suited for He. Reference [38] discussed the resonant levels of He (the n^1P series) where the onset of collision transfer processes [20,34] occurs at pressures well below the value where radiation trapping has begun to reach its asymptotic value. This difficulty, however, is due to some of the peculiarities of helium, rather than being a general problem with the technique of complete radiation trapping. The resonant transitions of He have much smaller photon absorption cross sections than the resonant levels of the heavier rare gases, which shifts the critical pressure for radiation trapping to well over 10 mTorr. Furthermore, the near degeneracy ($\Delta E < 50$ cm^{-1}) of the He n^1P levels with the n^1D and n^1F levels (for $n \geqslant 4$) lead to very large excitation transfer cross sections that shift the onset of collision transfer effects to pressures at or below 20 mTorr. In contrast, we have found that for the heavy rare-gas levels we have studied the excitation transfer cross sections are in almost all instances small enough to have insignificant effects below 20 mTorr (see Sec. IV B). Thus, for the heavy rare gases the pressure for secondary processes are generally well above the critical pressure for radiation trapping. By exploiting this gap, it is possible to take measurements at moderate pressures and use the Heddle model to extrapolate the results to higher pressures where measurements would be difficult.

ACKNOWLEDGMENTS

This work was supported by the Air Force Office of Scientific Research and the National Science Foundation.

[1] R. D. Cowan, *The Theory of Atomic Structure and Spectra* (University of California Press, Berkeley, 1981).
[2] T. Holstein, Phys. Rev. **72**, 1212 (1947).
[3] G. Herzberg, *Atomic Spectra and Atomic Structure* (Dover, New York, 1945).
[4] A. C. G. Mitchell and M. W. Zemansky, *Resonance Radiation and Excited Atoms* (Cambridge University Press, London, 1961).
[5] P.J.M. van der Burgt, W.B. Westerveld, and J.S. Risley, J. Phys. Chem. Ref. Data **18**, 1757 (1989).
[6] I. Kanik, J.M. Ajello, and G.K. James, J. Phys. B **29**, 2355 (1996).
[7] J.M. Ajello, G.K. James, B. Franklin, and S. Howell, J. Phys. B **23**, 4355 (1990).
[8] S. Tsurubuchi, K. Arakawa, S. Kinokuni, and K. Motohashi, J. Phys. B **33**, 3713 (2000).
[9] S. Tsurubuchi, T. Miyazaki, and K. Motohashi, J. Phys. B **29**, 1785 (1996).
[10] K.H. Tan, F.G. Donaldson, and J.W. McConkey, Can. J. Phys. **52**, 786 (1974).
[11] J.W. McConkey and F.G. Donaldson, Can. J. Phys. **51**, 914 (1973).
[12] M.H. Phillips, L.W. Anderson, and C.C. Lin, Phys. Rev. A **32**, 2117 (1985).
[13] J.E. Chilton, J.B. Boffard, R.S. Schappe, and C.C. Lin, Phys. Rev. A **57**, 267 (1998).
[14] J.T. Fons and C.C. Lin, Phys. Rev. A **58**, 4603 (1998).
[15] A.H. Gabriel and D.W.O. Heddle, Proc. R. Soc. London, Ser. A **258**, 124 (1960).
[16] D.W.O. Heddle and M.J. Samuel, J. Phys. B **3**, 1593 (1970).
[17] J.E. Chilton, M.D. Stewart, and C.C. Lin, Phys. Rev. A **62**, 032714 (2000).
[18] J.E. Chilton, M.D. Stewart, and C.C. Lin, Phys. Rev. A **61**, 052708 (2000).
[19] A.R. Filippelli, C.C. Lin, L.W. Anderson, and J.W. McConkey, Adv. At., Mol., Opt. Phys. **33**, 1 (1994).
[20] J.E. Chilton and C.C. Lin, Phys. Rev. A **58**, 4572 (1998).
[21] T. Holstein, Phys. Rev. **83**, 1159 (1951).
[22] A.V. Phelps, Phys. Rev. **110**, 1362 (1958).
[23] J.E. Chilton and C.C. Lin, Phys. Rev. A **60**, 3712 (1999).
[24] C.E. Theodosiou, At. Data Nucl. Data Tables **36**, 98 (1987).
[25] M. Aymar and M. Coulombe, At. Data Nucl. Data Tables **21**, 537 (1978).
[26] NIST Atomic Spectra Database, URL http://physics.nist.gov/asd
[27] R.A. Lilly, J. Opt. Soc. Am. **66**, 245 (1976).
[28] M.J. Seaton, J. Phys. B **31**, 5315 (1998).
[29] V.E. Bubelev and A.N. Grum-Grzhimailo, J. Phys. B **24**, 2183 (1991).
[30] J.B. Boffard, G.A. Piech, M.F. Gehrke, L.W. Anderson, and C.C. Lin, Phys. Rev. A **59**, 2749 (1999).
[31] B.L. Moiseiwitch and S.J. Smith, Rev. Mod. Phys. **40**, 238 (1968).
[32] C.A. DeJoseph and J.D. Clark, J. Phys. B **23**, 1879 (1990).
[33] D.W.O. Heddle and C.B. Lucus, Proc. R. Soc. London, Ser. A **271**, 129 (1963).
[34] A.F.J. van Raan and J. van Eck, J. Phys. B **7**, 2003 (1974).
[35] W.B. Westerveld and J. van Eck, J. Quant. Spectrosc. Radiat. Transf. **17**, 131 (1977).
[36] J.E. Mentall and H.D. Morgan, Phys. Rev. A **14**, 954 (1976).
[37] L.R. Peterson and J.E. Allen, J. Chem. Phys. **56**, 6068 (1972).
[38] D.W.O. Heddle and J.W. Gallagher, Rev. Mod. Phys. **61**, 221 (1989).